arXiv:1609.09361v1 [astro-ph.HE] 29 Sep 2016

Microphysics in the gamma ray burst central engine

Agnieszka Janiuk[1]

[1] *Center for Theoretical Physics, Polish Academy of Sciences, Al. Lotnikow 32/46, 02-668 Warsaw, Poland*

agnes@cft.edu.pl

ABSTRACT

We calculate the structure and evolution of a gamma ray burst central engine where an accreting torus has formed around the newly born black hole. We study the general relativistic, MHD models and we self-consistently incorporate the nuclear equation of state. The latter accounts for the degeneracy of relativistic electrons, protons, and neutrons, and is used in the dynamical simulation, instead of a standard polytropic γ-law. The EOS and provides the conditions for the nuclear pressure in the function of density and temperature, which evolve with time according to the conservative MHD scheme. We analyze the structure of the torus and outflowing winds, and compute the neutrino flux emitted through the nuclear reactions balance in the dense and hot matter. We also estimate the rate of transfer of the black hole rotational energy to the bipolar jets. Finally, we elaborate on the nucleosynthesis of heavy elements in the accretion flow and the wind, through computations of the thermonuclear reaction network. We suggest that the observable signatures of the radioactive elements decay in the accretion flow may help constrain the black hole mass and spin, as complementary to the gravitational wave analysis.

Subject headings: black hole physics; gamma ray bursts; MHD

1. Introduction

Gamma Ray Bursts (GRB), are extremely energetic transient events, visible from the most distant parts of the Universe. When a newly born black hole forms, either via the core collapse supernova, or after the merger of two compact stars, a large amount of matter is accreted onto it within the timescale between tens of milliseconds, to thousands of seconds, with a highly hyper-Eddington rates (Woosley 1993; Paczynski 1998). In such conditions,

the nuclear reactions inside the plasma lead to creation of neutrinos, mainly via the electron-positron capture on nucleons. The annihilation of neutrino-antineutrino pairs is a source of power to the relativistic jets launched along the axis of the disk-black hole system. This can be comparable to the power extracted on the cost of the black hole spin, with the disk mediated by the magnetic fields. Both neutrinos and magnetic fields in the accreting matter can drive the wind outflow from the disk surface, and act as a collimation mechanism for the relativistic jets (see, e.g., Lee & Ramirez-Ruiz (2007) and references therein). The latter, are then the sites of the high-energy radiation produced at large distances from the engine, on the cost of the magnetic reconnection and conversion of the jet electromagnetic energy flux into heat (e.g., Bromberg & Tchekhovskoy (2016)).

In the outer parts of the disc, the heavy elements can be formed, and then the isotopes are prone to the radioactive decay (Fujimoto et al. 2004). This may in the future bring observable effects on the measured hard X-ray spectra of GRBs (Janiuk 2014) as well as the additional peaks in the blue and infrared bands a few days after the prompt GRB emission (Martin et al. 2015). In addition, the gamma ray bursts contribute in this way to the galactic chemical evolution (Surman et al. 2014). The physical conditions in this engine, its density, temperature, and electron fraction, depend on the global parameters of the flow, such as the amount of matter and accretion rate, black hole mass and its spin, and the magnetic field. These conditions in turn will affect the total abundances of heavier elements synthesized within the flow. Therefore, a possible detection of weak gamma ray burst signatures, apart from its gamma ray fluence, could give a constraint on the black hole parameters. These, in turn, can now be independently estimated, if the black hole is born via a merger event, detectable in the gravitational wave interferometer.

Numerical computations of the structure and evolution of the accretion flow in the gamma ray bursts engine begun with steady-state, and time-dependent models, which were axially and vertically averaged, and based on the classical prescription for visocisty with the so-called α-parameter (Popham et al. 1999; Di Matteo et al. 2002; Kohri & Mineshige 2002; Kohri et al. 2005; Reynoso et al. 2006; Chen & Beloborodov 2007; Janiuk et al. 2004, 2007; Janiuk & Yuan 2010). More recently, these accretion flows are being described by fully relativistic, MHD computations (Barkov & Komissarov 2010; Barkov & Baushev 2011; Janiuk et al. 2013; Kyuchi et al. 2015).

In this work, we study the central engine of a gamma ray burst, which is composed of a stellar mass, rotating black hole and accreting torus that has formed from the remnant matter at the base of the GRB jet. We compute the time-dependent, two dimensional model of the rotationally supported, magnetized disc, rapidly accreting onto the center. The simulation is based on the HARM (High Accuracy Magnetohydrodynamics) scheme, which works on the

stationary metric around black hole and integrates the total energy equation and updates the set of 'conserved' variables, i.e. comoving density, energy-momentum, magnetic field (Gammie et al. 2003).

The basic version of the HARM scheme was designed to model the accretion flows in the centers of galaxies, where the gas equation of state is with a good accuracy that of an ideal gas and can be described usin an adiabatic relation (e.g., Moscibrodzka & Falcke (2013)). In our current dynamical model, we use the non-ideal equation of state, computed on the basis of the β-equilibrium (Janiuk et al. 2007). We allow for the partial degeneracy of relativistic nucleons, electrons and positrons in the accreting plasma, and we compute the neutrino cooling rate due to the weak interaction processes, electron-positron pair anihillation, as well as bremsstrahlung and plasmon decay. Here, we first incorporate this detailed microphysics into the heart of the GR MHD scheme. The neutino cooling was computed already from the nuclear reaction balance in the context of gamma ray bursts in our previous work (Janiuk et al. 2013). However, in that work, still the simple, adiabatic relation for the pressure ($P = (\gamma-1)u$, with $\gamma = 4/3$) was used, and only the internal energy in the evolution was updated during the simulation. In the current model, we mainly address the question of microphysics in the accretion flow, and also we are now able to more self-consistently estimate the efficientcy of the neutrino cooling in the disk. We check, if it is capable of powering the relativist jets in the gamma ray bursts, now in the case of a rather weak magnetic field. We also check the effect of the rotation speed of the black hole. In addition, we analyze the structure, velocity and amount of mass loss through the uncollimated winds launched from the accretion disc. Finally, we examine the resulting nucleosynthesis in the body of the disk, which can occur already at small distances from the black hole, as well as in the uncollimated winds, and we show that the accretion flow can be the site of significant heavy element production.

The article is organized as follows. In § 2, we describe our MHD model of the GRB central engine. In § 3, we present the results, describing the structure of the torus and the effects of adopted microphysics treatment. We also discuss the power transferred to the jets via the neutrino anihillation in comparison with the energy extracted to power the GRB jets from the magnetic fields dragged through the BH horizon. In § 4 we describe the process of heavy elements formation in the outskirts of the torus in the GRB central engine. We present the resulting abundances of elements computed under the assumption of nuclear statistical equilibrium. Finally, we compare our results with the previous simulations. We discuss the results in § 5.

2. Model of the hyperaccreting disk

The model computations are based on the axisymmetric, general relativistic MHD code *HARM-2D*, described by Gammie et al. (2003) and Noble et al. (2006). It uses a conservative, shock-capturing scheme, and provides solver for the continuity and energy-momentum conservation equations, assuming a force-free approximation. Here we use our own version of this code, which we supplemented with the numerical routines to compute the equation of state and rate of cooling by neutrinos.

2.1. Equation of state and neutrino cooling

The neutrino cooling processes adopted in our computations are the reactions of electron and positron capture on nucleons, the electron-positron pair anihillation, nucleon bremsstrahlung and plasmon decay. These reactions are:

$$\begin{aligned} p + e^- &\rightarrow n + \nu_{\rm e} \\ p + \bar{\nu}_{\rm e} &\rightarrow n + e^+ \\ p + e^- + \bar{\nu}_e &\rightarrow n \\ n + e^+ &\rightarrow p + \bar{\nu}_{\rm e} \\ n &\rightarrow p + e^- + \bar{\nu}_{\rm e} \\ n + \nu_{\rm e} &\rightarrow p + e^- \end{aligned} \tag{1}$$

and their reaction rates are given by appropriate integrals (Reddy et al. 1998; Janiuk et al. 2007) In addition, the neutrinos are produced due to the electron-positron pair anihillation, bremsstrahlung, plasmon decay, in the following reactions:

$$e^- + e^+ \rightarrow \nu_{\rm i} + \bar{\nu}_{\rm i} \tag{2}$$

$$n + n \rightarrow n + n + \nu_{\rm i} + \bar{\nu}_{\rm i} \tag{3}$$

$$\tilde{\gamma} \rightarrow \nu_{\rm e} + \bar{\nu}_{\rm e} \tag{4}$$

We calculate their rates numerically, with proper integrals over the distribution function of relativistic, partially degenerate species. Finally, the total neutrino cooling rate is given by the two-stream approximation (Di Matteo et al. 2002), and includes the scattering and absorptive optical depths for neutrinos of the three flavors:

$$Q_\nu^- = \frac{\frac{7}{8}\sigma T^4}{\frac{3}{4}} \sum_{i=e,\mu,\tau} \frac{1}{\frac{\tau_{{\rm a},\nu_{\rm i}}+\tau_{\rm s}}{2} + \frac{1}{\sqrt{3}} + \frac{1}{3\tau_{{\rm a},\nu_{\rm i}}}} \times \frac{1}{H} \tag{5}$$

and is expressed in the units of erg $s^{-1}cm^{-3}$.

The structure of a magnetized accreting torus in which the above reactions take place and the gas looses energy via neutrino cooling, was investigated in our previous paper (Janiuk et al. 2013). In that work, however, the neutrino cooling rate was used to update in every time step only the internal energy in the plasma, and the pressure was still approximately computed from the adiabatic relation, $p = (\gamma - 1)e$, with constant $\gamma = 4/3$, which simplifies a lot the GR MHD scheme.

The leptons and baryons are relativistic in the GRB engine, and may have an arbitrary degeneracy level, so we compute the gas pressure using the Fermi-Dirac distribution of the species. Also, neutrinos may contribute to the pressure due to the fact that they are scattered and absorbed, similarly to the photons and (rather negligibly small in the GEB case) radiation pressure component. In the total pressure, we include now the contributions from the free nucleons, pairs, radiation, trapped neutrinos, and also from the Helium nuclei.

$$P_{\rm gas} = P_{\rm nucl} + P_{\rm He} + P_{\rm rad} + P_{\nu} \tag{6}$$

where $P_{\rm nucl}$ includes free neutrons, protons, and the electron-positrons:

$$P_{\rm nucl} = P_{\rm e-} + P_{\rm e+} + P_{\rm n} + P_{\rm p} \tag{7}$$

with

$$P_{\rm i} = \frac{2\sqrt{2}}{3\pi^2}\frac{(m_i c^2)^4}{(\hbar c)^3}\beta_i^{5/2}\left[F_{3/2}(\eta_{\rm i},\beta_{\rm i}) + \frac{1}{2}\beta_{\rm i}F_{5/2}(\eta_{\rm i},\beta_{\rm i})\right]. \tag{8}$$

Here, $F_{\rm k}$ are the Fermi-Dirac integrals of the order k, and $\eta_{\rm e}$, $\eta_{\rm p}$ and $\eta_{\rm n}$ are the reduced chemical potentials, $\eta_i = \mu_i/kT$, is the degeneracy parameter, where μ_i the standard chemical potential. Reduced chemical potential of positrons is $\eta_{\rm e+} = -\eta_{\rm e} - 2/\beta_{\rm e}$. Relativity parameters are defined as $\beta_{\rm i} = kT/m_{\rm i}c^2$. The total pressure is computed numerically by solving the balance of nuclear reactions (Yuan 2005; Janiuk & Yuan 2010).

2.2. Initial conditions and dynamical model

The numerically computed nuclear EOS is incorporated now into the MHD scheme, with the pressure computed as a function of density and temperature. The MHD scheme solves for the inversion between the so called 'primitive' and 'conserved' variables at every time-step (see e.g., Noble et al. 2006). The code HARM-2D provides solver for continuity and energy-momentum conservation equations:

$$(\rho u^{\mu})_{;\mu} = 0 \tag{9}$$

$$T^{\mu}{}_{\nu;\mu} = 0 \tag{10}$$

where:

$$\begin{aligned} T^{\mu\nu} &= T^{\mu\nu}_{\rm gas} + T^{\mu\nu}_{\rm EM} \\ T^{\mu\nu}_{\rm gas} &= \rho h u^\mu u^\nu + p g^{\mu\nu} = (\rho + u + p) u^\mu u^\nu + p g^{\mu\nu} \\ T^{\mu\nu}_{\rm EM} &= b^2 u^\mu u^\nu + \frac{1}{2} b^2 g^{\mu\nu} - b^\mu b^\nu; \quad b^\mu = u_\nu {}^*F^{\mu\nu} \end{aligned} \tag{11}$$

and u^μ is the four-velocity of gas, u is the internal energy density, $b^\mu = \frac{1}{2}\varepsilon^{\mu\nu\rho\sigma} u_\nu F_{\rho\sigma}$ is the magnetic four-vector, and F is the electromagnetic stress tensor. Assuming the force-free approximation, we have $E_\nu = u_\mu F^{\mu\nu} = 0$.

The conservative numerical scheme which is used in this code, in general solves $\partial_t \mathbf{U}(\mathbf{P}) = -\partial_i \mathbf{F}^i(\mathbf{P}) + \mathbf{S}(\mathbf{P})$ where $\mathbf{U}$ is a vector of "conserved" variables (momentum, energy density, number density, taken in the coordinate frame), $\mathbf{P}$ is a vector of 'primitive' variables (rest mass density, internal energy), $\mathbf{F}^i$ are the fluxes, and $\mathbf{S}$ is a vector of source terms.

In contrast to the non-relativistic MHD, where $\mathbf{P} \to \mathbf{U}$ and $\mathbf{U} \to \mathbf{P}$ have a closed-form solution, in relativistic MHD, $\mathbf{U}(\mathbf{P})$ is a complicated, nonlinear relation. Inversion $\mathbf{P}(\mathbf{U})$ is calculated therefore, in every time step, numerically. The inverse transformation requires to solve a set of 5 non-linear equations, which is done by a multi-dimensional Newton-Raphson routine. The procedure is simple, if the pressure is given by an adiabatic relation with density. However, for a general equation of state, one must compute also dp/dw, dp/dv^2, and $p(W, v^2, D)$ (here we have enthalpy, $w = p + u + \rho$; $W = \gamma^2 w$; $D = \sqrt{-g}\rho u^t$). In our scheme, we have tabulated pressure and internal energy as a function of density and temperature, $(p, u)(\rho, T)$, and we interpolate over this table. In addition, density and temperature in the flow give us a unique determination of the neutrino cooling rate. The Jacobian $\partial\mathbf{U}/\partial\mathbf{P}$ is computed numerically, and the conserved variables are evolved in time. To speed up the computations, our version of this code was parallelized using the MPI technique, for the hydro-evolution, and we also implemented the shared memory hyper-threading for the EOS-table interpolation.

The simulations are conducted in 2D, on the spherical grid with the resolution of 256x256 cells in the r and θ directions, and typically run up to t=2000-3000 M. The grid is spaced logarithmically in radius and concentrated towards the equatorial plane, defined as in Gammie et al. (2003).

The initial conditions for the accretion flow are given by the equilibrium torus solution, defined as in (Fishbone & Moncrief 1976) and Abramowicz et al. (1978). The parameters of the model are the black hole mass and its spin. The torus mass is defined by the radius

of the pressure maximum, and it is also supplemented with the density scaling, which is necessary to compute the pressure and temperature in the torus in physical units. The model is seeded by the initial magnetic field. The magnetic field in our current computations is adopted to have a standard, poloidal configuration given with the ϕ-component of its vector potential scaling with the density, $A_\phi = (\rho/\rho_{max})$, and is weakly magnetized, with an initial $\beta = P_{\rm gas}/P_{\rm mag} = 50$ (see e.g., McKinney, Tchekhovskoy & Blandford (2012) for the discussion of various other field configurations).

3. Structure of the flow

3.1. Accreting torus and wind outflow

The initial conditions introduced from the pressure equilibrium solution are relaxed after about $1000M$ (in dimensionless units, with $G = c = 1$), and then the flow is evolves to the form the dynamically driven, geometrically thin flow, which is accreting through the black hole horizon. In the example Figure 1, we plot the radial profiles of the torus thickness for the cooled torus, at four time snapshots. The initial condition represents the equilibrium torus (a 'doughnut') and this profile spreads with time into larger radii. The torus thickness is computed from the pressure scale-height, as follows

$$H_{\rm d} = \frac{1}{\Omega} c \sqrt{\frac{P}{\rho c^2 + e}}, \tag{12}$$

where $\Omega = \frac{c^3}{GM} \frac{1}{(a+r^{3/2})}$ is the Keplerian frequency and the sound speed is approximately given by its relativistic form as above (see Ibanez et al. (2015)). The thickness of the torus is about $H/r \sim 0.2$. The exact value depends on the black hole spin, both in the initial equilibrium and time-dependent solution. The maximum thickness of the torus, defined as above, reaches from 7 to 9 $r_{\rm g}$ in the initial model, for the spins from 0.6, to 0.98. The maximum thickness at the time $t = 2000M$ increases to about 10-14 $r_{\rm g}$, for this range of spins. Also, as the Figure 1 shows, it is shifted to the outer boundary, while the torus no longer keeps its equilibrium 'doughnut' shape.

In Figure 2 we plot the accretion rate through the black hole horizon in the function of time. The mean rate of accretion is about 0.3-0.4 $M_\odot$ s^{-1}, for the black hole mass of 3 $M_\odot$, depending slightly on the black hole spin (see Table 1). The instantaneous peaks which appear in the flaring states, reach the values up to several Solar mass per second. These flares disappear as the initial condition is evolved, and then the accretion rate varies only by a few per cent.

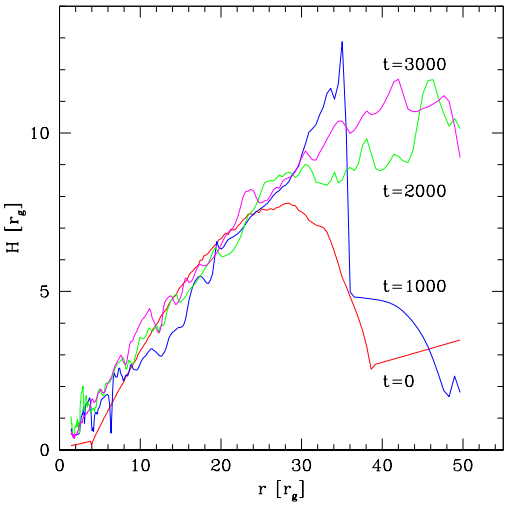

Fig. 1.— Thickness of the torus in the function of radius, at four different time snapshots during the simulation, t=0, 1000, 2000, and 3000 M, as labelled in the plot and marked by different colors. The model includes numerical EOS and neutrino cooling. Parameters of the model are $M_{\rm BH} = 3M_\odot$, $M_{\rm torus} \approx 0.1M_\odot$. Black hole spin is $a = 0.9$.

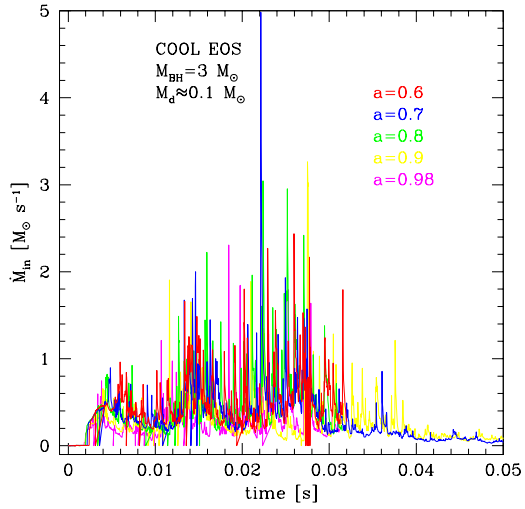

Fig. 2.— Accretion rate as a function of time, in the models with neutrino cooling. The models were calculated for a range of black hole spin parameters: a=0.6, 0.7, 0.8, 0.9, and 0.98, with red, blue, green, yellow, and magenta lines, respectively. The black hole mass is equal to $3M_\odot$, and the initial disk mass is about $0.1M_\odot$

In Figure 3 we show the two-dimensional maps of the torus structure, in the $r-\theta$ plane, obtained from the calculations in the model with the black hole mass of 3 $M_{\odot}$ and spin of $a = 0.6$. The snapshots from our simulation were taken at time $t = 2000M$, which for the adopted black hole mass is equivalent to about 0.03 s. The maps present the rest mass density ρ, gas temperature T, and magnetic pressure to gas pressure ratio β, over-plotted with magnetic field lines. We also show the distribution of the neutrino emissivities within the flow, as computed from the equation of state of the matter for these profiles of temperature and density. The last panel to the right in Figure 3, presents the velocity field in the flow. The arrows (normalized length) show the direction of velocity, while the color map presents the ratio of the flow velocity to the speed of light, $v/c = \sqrt{g^{\mu\nu}u^{\mu}u^{\nu}}$. The turbulent velocity field in the torus is changing into a uniform outflow that is launched above the torus surface at high latitudes.

The disk winds are sweeping the gas out from the system, both in the equatorial plane and at higher latitudes. We identified the regions of the wind in the computation domain by defining three conditions that must be satisfied simultaneously, to distinguish the wind from the torus main body, and from the magnetized jets: (i) the radial velocity of the plasma is positive (ii) the density is smaller than 10^9 g cm^3 and (iii) the gas pressure is dominant, $\beta > 1.0$. The winds are located approximately at radii above 10 $R_{\rm g}$ and latitudes between about $30^{\circ}-60^{\circ}$ and $120^{\circ}-150^{\circ}$. The velocity in the wind is typically $v/c \sim 0.06-0.5$, and its maximum value is only slightly depending on the black hole spin. The density in the wind, by definition, is below 10^9 g sm^{-3}, but may drop down to 10^5 g cm^{-3}. The temperature of the wind in the neutrino cooled models is in the range of $6 \times 10^9 - 5.7 \times 10^{10}$ K. Such high temperatures, above the threshold for electron-positron pair production, $T = m_{\rm e}c^2 \approx 5 \times 10^9$ K, are the key condition for neutrino emission processes. The neutrino cooling is then efficient, as it only weakly depends on density. In the clumps with $\rho >\sim 10^8$ g cm^{-3}, the nuclear processes lead to neutrino production, while the optical depths for their absorption are very small.

The effect of the wind is the mass loss from the system. We estimated quantitatively the evolution of the mass during the simulation. The total mass removed from the torus during the simulation, calculated by integrating the density over the total volume, differs from the total mass accreted onto the black hole (i.e. the time integrated mass accretion rate through the inner boundary, subtracted from the initial mass). This may depend on the black hole spin. For the model with $a = 0.6$, the simulation was ended when the total mass in the volume dropped below $0.089M_{\odot}$. The starting mass at $t = 0$, was equal to $0.11M_{\odot}$. During the simulation, about 0.014 Solar masses was accreted onto the black hole (which makes 20% of the initial mass), and the rest, about 6%, was lost from the computation domain in the outflows. For larger black hole spins, the fraction of mass lost through wind can reach about

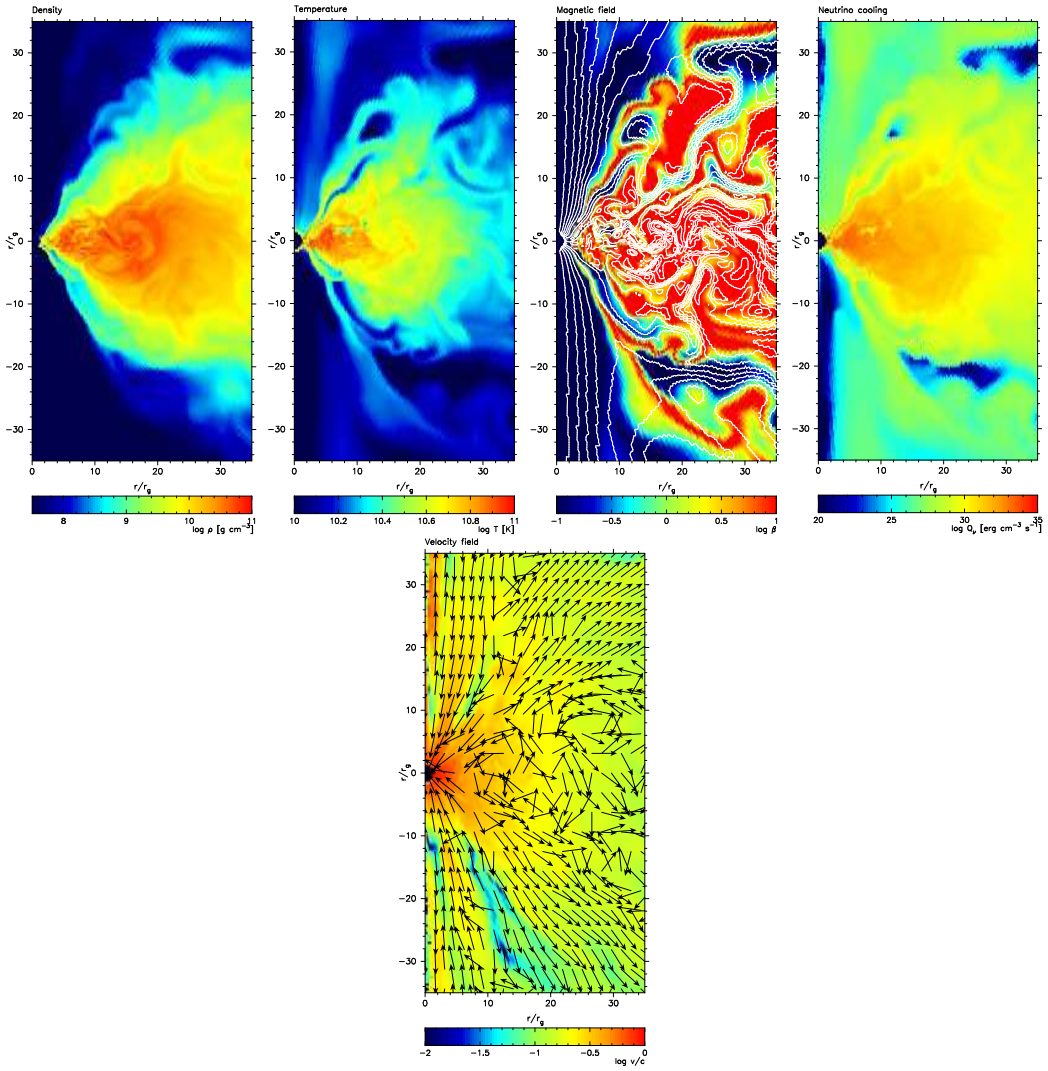

Fig. 3.— Structure of accretion disk at the end of the simulation. The model accounts for the neutrino cooling and nuclear EOS. The maps show: (i) density, (ii) temperature of the plasma, (iii) ratio of gas to magnetic pressure, with field lines topology, (iv) neutrino emissivity Q_ν, and (v) velocity field (from left to right). The snapshots are taken at time t=2000 M, which is equivalent to $t \approx 0.03$ s. Parameters of the model: black hole mass $M_{\rm BH} = 3M_\odot$, torus mass $M_{\rm t} = 0.1M_\odot$, and BH spin $a = 0.6$.

10%. The values for all the models are collected in Table 1.

The hot, magnetized, transient polar jets appear as well, and they form on both sides of the black hole, as can be seen in the maps in Figs. 3. They are present in a narrow region along the polar axis, where the open magnetic field lines have formed. Velocity field is directed there outwards, and the gas is expelled from the black hole region with the velocity that is nearly at the speed of light.

3.2. Neutrino luminosity and Blandford-Znajek energy extraction

The total neutrino luminosity in the function of time is shown in Figure 4, where we present the results for the black hole mass of 3 $M_\odot$ and torus of $\approx 0.1 M_\odot$. The luminosities are plotted for a range of black hole spins: $a = 0.6, 0.7, 0.8, 0.9$, and 0.98. Initially, the total integrated neutrino luminosity is in the range 6×10^{52}-2×10^{53} erg s^{-1}, and temporarily drops, when the matter starts accreting. As the initial state is evolved, the luminosity grows to over 10^{53} erg s^{-1} and at time $t = 0.03$ s reaches roughly a constant level, scaling with the black hole spin. The exact values of L_ν at the end of the simulation are given in Table 1.

The neutrinos are emitted from the torus as well as from the hot, rarefied wind. The wind contribution to the total luminosity is of about 10-11% for all the models. The luminosity of the densest parts of the torus, estimated by weighing the total emissivity by the plasma density, is only on the order of $10^{48} - 10^{49}$ erg s^{-1}. This is because the total opacity for neutrino absorption and scattering in this regions reaches $\tau \sim 1 - 5$. and the neutrinos are trapped in the dense plasma.

The power and luminosity available through the Blandford-Znajek process (Blandford & Znajek 1977) is calculated from the electromagnetic stress tensor, given by

$$T^{\mu\nu}_{\rm EM} = b^2 u^\mu u^\nu + \frac{b^2}{2} g^{\mu\nu} - b^\mu b^\nu, \tag{13}$$

where b^μ is the magnetic four-vector, with $b^t = g_{i\mu} B^i u^\mu$ and $b^i = (B^i + u^i b^t)/u^t$ and u^μ is the four-velocity. We compute the radial electromagnetic flux through the horizon as in (McKinney & Gammie 2004):

$$\dot{E} = 2\pi \int_0^\pi d\theta \sqrt{-g} F_{\rm EM}, \tag{14}$$

where $F_{\rm EM} = -T^r_t$ and g is the metric determinant. We consider only the flux, which is dragged inwards through the black hole horizon, and we also check the magnetization of the plasma there, $\beta(r_{\rm in}) = B^2/\rho(r_{\rm in})$, where ρ is the rest mass density of the gas. We impose a condition of $\beta(r_{\rm in}) \geq 1.0$, otherwise the Blandford-Znajek power is set to be zero.

The resulting BZ luminosities in the function of time for the range of black hole spin values in different models are presented in Figure 5. As the Figure shows, the continuous power supply to the jet on the order of above 10^{52} erg s^{-1} is available only for the highly spinning black holes. If the spin is moderate, $a = 0.6 - 0.8$, then the power $L_{\rm BZ} \approx 10^{51}$ erg s^{-1} is injected. Episodically, the power drops to zero, when there is no magnetization on the black hole horizon. Therefore, the power injection can be separated by the intervals of the 'BZ-quiescence', which can be longer if the black hole spin is small.

The exact values of the BZ-luminosity at the end of the simulations are given in Table 1.

3.3. Comparison to the models without neutrino cooling

To quantify the effect of microphysics, equation of state, and the neutrino cooling in 2D MHD simulations, we ran a set of test models with no cooling and adiabatic equation of state with $\gamma = 4/3$, as in the standard HARM models. The model parameters and initial conditions were otherwise the same.

In Figure 6 we plot the rate of matter accretion through the inner boundary, as a function of time for a set of models with various black hole spins. The average accretion rate onto black hole is slightly lower in the adiabatic models than in the cooled models, for the same model parameters. The initial conditions are evolved slower in the adiabatic case, and the flaring peaks in the accretion rate appear for a longer time. The highest peak in this set of models appeared for $a = 0.6$, and not for $a = 0.7$, which was the case in the neutrino cooled torus. The quasi-stationary, almost constant accretion rate value, appears after $t \approx 0.04$, and the mean value of the accretion rate is on the same order as in neutrino cooled models, but somewhat lower (see Table 1 for exact values).

In the adiabatic models, the neutrino luminosity is set to zero, by definition. The only source of the energy extraction and power supply to the jets is therefore the rotation of the black hole and magnetic flux. In Figure 7 we show the Blandford-Znajek luminosity in the function of time for this et of models, with various spins. We note that for the highest black hole spins, $a = 0.9 - 0.98$, the BZ luminosity is equally large as for the neutrino cooled tori, and it is almost constant with time. However, for the models with black hole spins of $a = 0.6 - 0.8$, the BZ power drops later in the evolution, and after $t \approx 0.02$ it is smaller than about 10^{50} erg s^{-1}. In other words, the energy extraction from the moderately rotating black hole by magnetic fields is less efficient, when the torus is not cooled by neutrinos.

The maps of the density, temperature, velocity and magnetic field in the exemplary

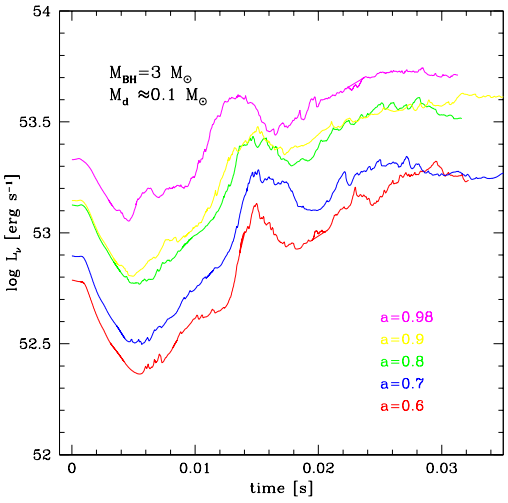

Fig. 4.— Total neutrino luminosity as a function of time. The black hole mass is $M_{\rm BH} = 3M_\odot$ and torus initial mass is $M_{\rm d} \sim 0.1M_\odot$. The models were calculated for a range of black hole spin parameters, $a = 0.98, 0.9, 0.8, 0.7$, and 0.6, as marked with magenta, yellow, green, blue, and red lines, respectively.

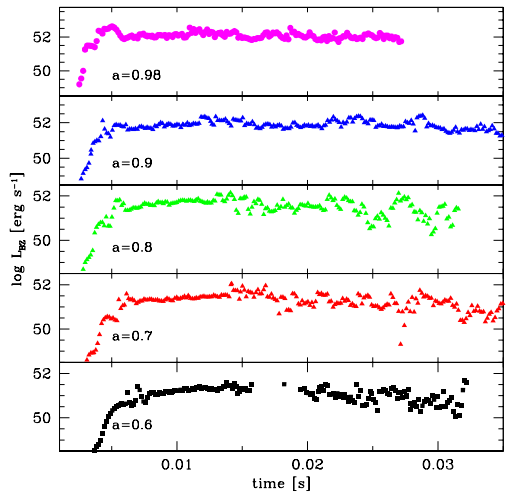

Fig. 5.— Power extracted from the black hole rotation through Blandford-Znajek process, and resulting luminosity as a function of time. The model includes numerical EOS and neutrino cooling. Parameters of the model are $M_{\rm BH} = 3M_\odot$, torus mass $M_{\rm t} \approx 0.1M_\odot$. The black hole spin values are marked in the panels, and range from a=0.6, to a= 0.98, from bottom to top panels

Table 1: Summary of the models. Black hole mass is $3M_\odot$. The mass of the torus is given in $M_\odot$, accretion rate in $M_\odot \mathrm{s}^{-1}$, the time is in seconds, and luminosity in erg s^{-1}.

Model	a	$R_{\rm max}$	$t_{\rm end}$	$M_{\rm t}(t=0)$	$M_{\rm t}(t_{\rm end})$	$< \dot{M} >$	$\dot{M}(t_{\rm end})$	$\Delta M_{\rm wind}$	$L_\nu^{\rm tot}(t_{\rm end})$	$L_{\rm BZ}(t_{\rm en}$
sbhAc	0.6	11.8	0.028	0.11	0.082	0.49	0.30	0.012	1.69×10^{53}	1.83×1
sbhBc	0.7	11.0	0.029	0.10	0.072	0.45	0.29	0.014	1.67×10^{53}	2.99×1
sbhCc	0.8	10.5	0.029	0.12	0.086	0.46	0.35	0.018	3.40×10^{53}	5.45×1
sbhDc	0.9	9.75	0.028	0.10	0.075	0.31	0.22	0.015	3.62×10^{53}	2.59×1
sbhEc	0.98	9.1	0.028	0.11	0.083	0.28	0.20	0.017	5.25×10^{53}	6.6×1
sbhAnc	0.6	11.8	0.032	0.11	0.090	0.46	0.31	0.005	–	1.0×1
sbhBnc	0.7	11.0	0.031	0.10	0.084	0.37	0.18	0.004	–	2.8×1
sbhCnc	0.8	10.5	0.044	0.12	0.108	0.24	0.04	0.004	–	4.43×1
sbhDnc	0.9	9.75	0.041	0.10	0.089	0.23	0.177	0.003	–	2.52×1
sbhEnc	0.98	9.1	0.035	0.11	0.097	0.18	0.109	0.007	–	7.62×1

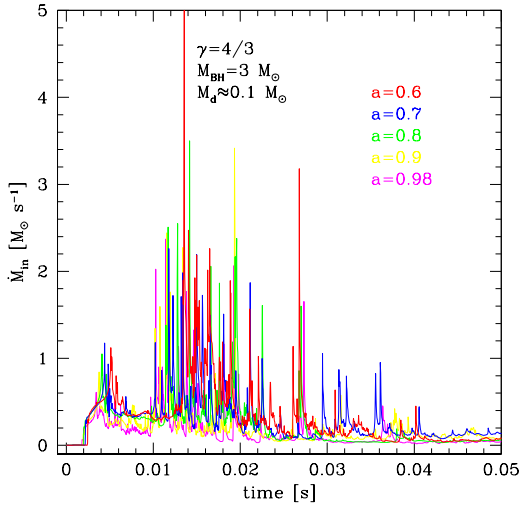

Fig. 6.— Accretion rate as a function of time, in the models without neutrino cooling, with polytropic EOS adopted with $\gamma = 4/3$. The values of black hole mass, spin, and disk mass are denoted in the figure.

model with $a = 0.6$, are shown in Figure 8. The density of the disk in the models without cooling is larger in the equatorial plane, while the disk seems to be compact (i.e., denser and geometrically thinner) close to the black hole. Due to the lack of neutrino cooling, it is also hotter than that presented in the Figure 3. The highest temperatures are achieved in the regions below 10 $r_{\rm g}$ in the disk, and also in the outflows (winds). Open magnetic field lines have formed, even for the small black hole spin, but in general the flow is less magnetized and the gas pressure is large bith in the disk and in the winds. The velocity field map shows the cooler, low density outflowing clumps, confined along the vertical axis.

The thickness of the torus, measured by the scale height given by Eq. 12 is shown in the Figure 9. In the adiabatic models, the disk is thicker geometrically, and at outer regions the ratio H/r saturates at the value of about 0.3-0.4. The mass loss rate is smaller than in the case of neutrino cooled tori, and typically only 1-3% of the torus mass is lost in the wind during the simulation. For the model with black hole spin close to maximal, $a = 0.98$, the total mass loss in the wind outflow is completely negligible, within our numerical accuracy.

4. Nucleosynthesis of heavy elements

In the astrophysical plasma, thermonuclear fusion occurs due to the capture and release of particles (n, p, α, γ). Reaction sequence produces further isotopes, and the set of non-linear differential equations is solved by Euler method (Wallerstein et al. 1999). The nuclear reactions may proceed with 1 (decays, electron-positron capture, photodissociacion), 2 (encounters), or 3 (triple alpha reactions) nuclei. Abundances of the isotopes are calculated under the assumption of nucleon number and charge conservation for a given density, temperature and electron fraction ($T \leq 1MeV$). Integrated cross-sections depending on temperature kT are determined with the Maxwell-Boltzmann or Planck statistics, and the background screening and degeneracy of nucleons must be taken into account.

We use the thermonuclear reaction network code *http://webnucleo.org*, and determine the relative abundances of heavy elements in the accreting torus. Given the density, temperature, and electron fraction, the *nuceq* library is used, and we compute the nuclear statistical equilibria established for the thermonuclear fusion reactions, taking the reaction rates available on JINA *reaclib* online database. This network is appropriate for temperatures below $1MeV$, which is the case at the outer radii of accretion disks in GRB engines. The mass fraction of the isotopes is solved for converged profiles of density, temperature and electron fraction in the disk, defined as:

$$Y_{\rm e} = \frac{n_{\rm e^-} - n_{e^+}}{n_{\rm b}}. \tag{15}$$

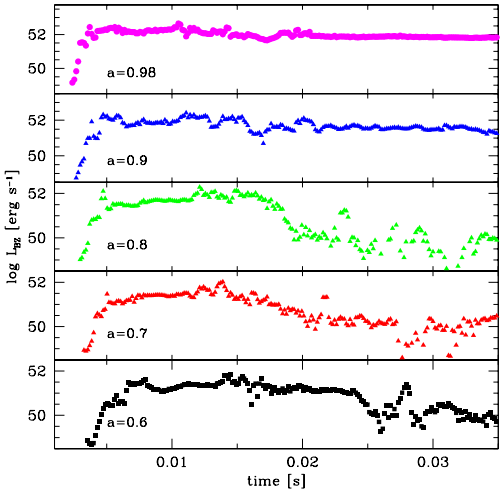

Fig. 7.— Power extracted from the black hole rotation through Blandford-Znajek process, and resulting luminosity as a function of time. The model is based o the adiabatic EOS, with $\gamma = 4/3$, and no neutrino cooling. Parameters of the model are $M_{\rm BH} = 3M_\odot$, torus mass $M_{\rm t} \approx 0.1M_\odot$. The black hole spin values are marked in the panels, and range from a=0.6, to a= 0.98, from bottom to top panels

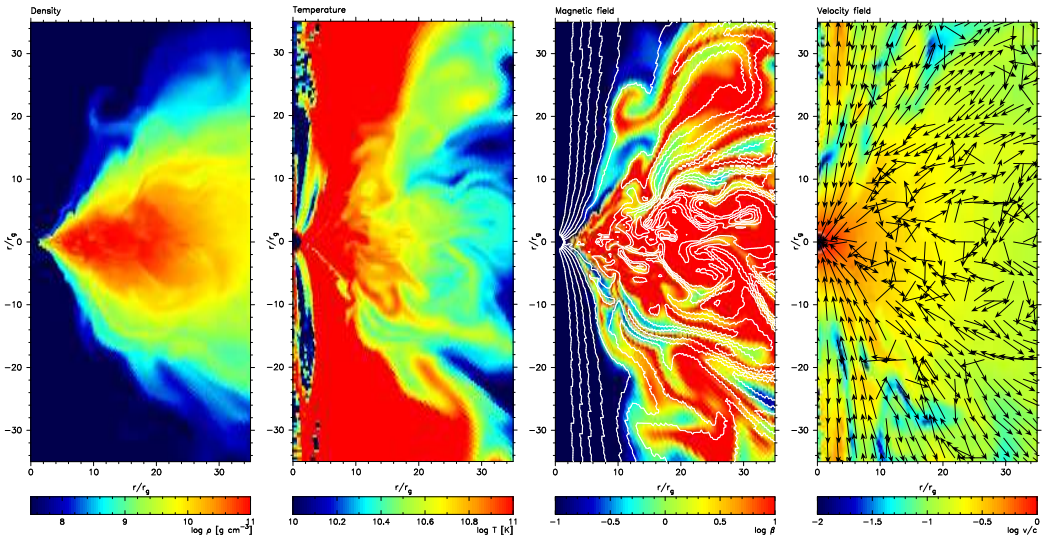

Fig. 8.— Model without neutrino cooling and with adiabatic equation of state. The parameters are: $a = 0.6$, $M_{\rm BH} = 3M_\odot$, $\beta_{\rm init} = 50$, torus mass $M_{\rm t} \approx 0.1M_\odot$. The maps, from left to right, show the distribution of density, temperature, ratio of gas to magnetic pressure with field lines topology, and velocity field. The snapshots are taken at $t = 2000M$, which is equivalent to $t \approx 0.03$ s of the dynamical simulation.

We use here a standard, publicly available software, and a more detailed description of our procedure can be found in Janiuk (2014).

In Figure 10 we plot the electron fraction in the 2-D maps of the accretion flow. The parameters of this simltaion were: the black hole of mass equal to $3M_{\odot}$, torus mass of about $0.11M_{\odot}$, and the black hole spins of 0.6 and 0.9, as shown in the left and right panels, respectively. Distributions are plotted at the evolved time of the simulation, for $t = 2000M$.

In Figure 11 we show the abundances of heavy elements, for these two models, which are produced in the torus and wind. The numbers are integrated up to the distance of $1000R_{\rm g}$ from the black hole. The first setup corresponds to a weak GRB scenario, as the power extracted from the black hole rotation is in this case of only about 10^{50} erg s^{-1}, and the total energy emitted by neutrinos is of about 10^{53} erg s^{-1}. Taking into account the efficiency of conversion of neutrino-antineutrino annihilation to the kinetic energy of the GRB jet, these two sources of power would result in a rather faint gamma ray burst. In this GRB engine, along with the abundant light elements such as Carbon, and then Silicon, Sulfur and Calcium isotopes, we expect also to find copious amounts of Titanium, Iron, and Nickel isotopes. The amount of the heavy elements decreases with time, and after about 0.02 second, the abundances of thses isotopes will drop by even 10-100 times.

The second setup corresponds to a bright GRB scenario, when the power available from the Blandford-Znajek process is 100 times higher, than in the first case, and also the power from the neutrino anihillation is almost 3 times higher. In this engine, similarly to the previous one, there will be produced isotopes of Iron and Vanadium, as well as Selenium, Manganese, Strontium, and Krypton. The latter are about 10 times more abundant, than in the case of a faint GRB engine, and they can be produced efficiently in the engine for a longer time.

5. Summary and discussion

We calculated the structure and short-term evolution of a gamma ray burst central engine in the form of a magnetized torus accreting onto a black hole. Our computations were performed in a fixed background metric around a spinning black hole, and the physical conditions in the plasma driven by the hyper-Eddington accretion rate were taken into account in the adopted microphysics. We describe the flow properties using the numerical equation of state of a dense and hot matter, where the free nucleons and electron-positron pairs are relativistic and partially degenerate. We estimate the resulting neutrino luminosity, which cools the flow via the nuclear reactions in which neutrinos of the three flavors

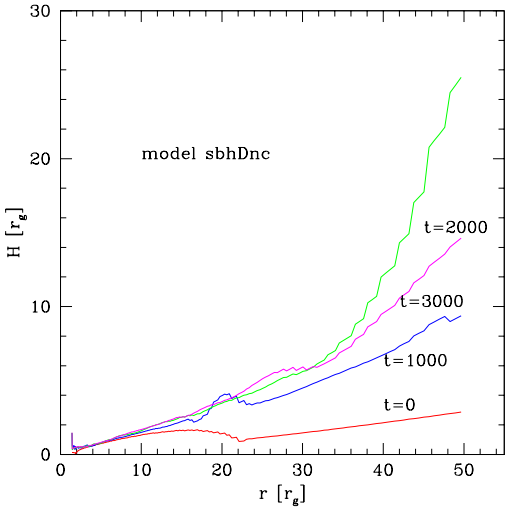

Fig. 9.— Thickness of the torus as a function of radius, in the models without neutrino cooling, with polytropic EOS adopted with $\gamma = 4/3$. The model is with the black hole spin $a = 0.9$.

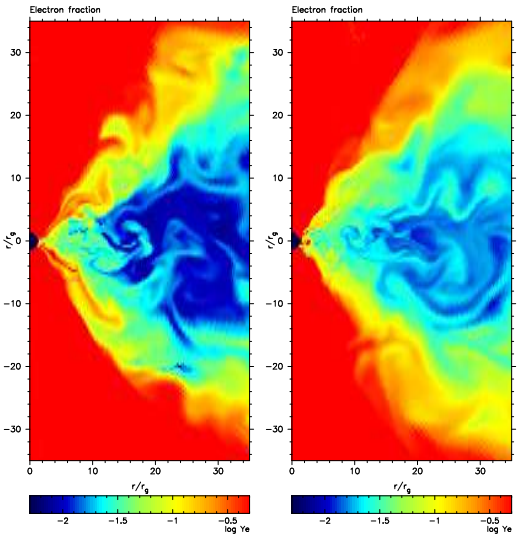

Fig. 10.— Electron fraction distribution. The snapshots are taken at $t = 2000M$. Models shown in the left and right panels are *sbhAc* and *sbhDc*, as labeled in the Table 1, respectively, and differ with the black hole spin.

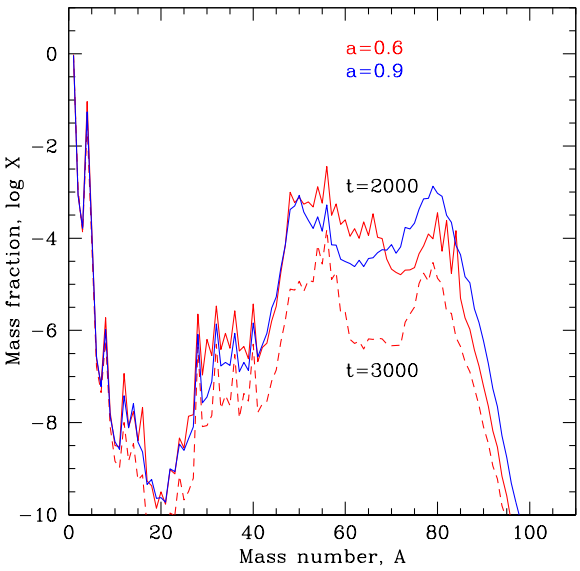

Fig. 11.— Volume integrated abundance distribution of elements synthesized in the accretion disk in 2D simulation with The black hole spin in the simulation was $a = 0.9$ (blue line), and $a = 0.6$ (red lines). The distributions of density, temperature, and electron fraction in the flow were taken at two time snapshots: $t = 2000M$ and $t = 3000M$, as marked with solid and dashed lines, respectively.

are produced. We conclude that the total integrated luminosity is larger than the power possibly extracted from the rotating black hole via the Blandford-Znajek process. Taking into account the uncertainty of the efficiency of the neutrino anihillation in the bi-polar jets (Zalamea & Beloborodov 2011), still we find that the power supply to the jets by neutrinos is plausibly competitive energetically with the magnetic flux extracting the black hole rotation energy. Finally, based on the computed structure of the flow, the density, temperature, and electron fraction, we estimate the integrated abundances of heavier elements which will be synthesized in the flow via subsequent reaction chain. These elements, if decaying radioactively at some distance from the central engine, will the contribute to the heating of the circum-burst medium, and afterglow emission.

As shown by Sekiguchi et al. (2015), the dynamical ejecta including neutrino transport may develop the shock waves, and related heating is responsible for enhanced reaction rates. The electron fraction is then increased, and their nuclear reaction networks are able to produce the r-process elements up to A=195. This was however not encountered in the Newtonian simulations, which produce elements up to A=130 (Goriely et al. 2011). Neutron star mergers are therefore expected to produce significant quantities of neutron-rich radioactive species, whose decay should result in a faint transient emission. The latter is called a 'kilonova', and should appear in the days following the burst. An observational support for such event has been reported e.g. by Tanvir et al. (2013) for a short duration GRB 130603B. The term refers to the luminosity peak in the near infrared band, rather than UV or Optical (Li & Paczynski 1998), and the emission produced in the regions of the opacities much higher than in the case of of supernovae.

The gamma ray bursts can play a unique role in the metal enrichment of the Universe, as they are the britest sources at all redshifts, and, for long GRBs, they occur in the star forming regions. Therefore, they provide an ideal probe of the effect of stellar evolution, on the galaxy chemical enrichment across the cosmic time. The ejecta created when the final explosive stages of the Population III stars provided the first elements beyond Helium into the surrounding interstellar medium, created seeds for the next generation of stars. Also, photons from these stars and radiation produced in the phase of accretion onto the first black holes, might contribute to the dissemination of first metals (see, e.g., Jonker et al. (2013)). Because the nucleosynthesis yields from the explosions of stars in different populations could differ by orders of magnitude, the metal abundance patterns, imprinted in the interstellar medium, should depend on the initial mass function. The primordial initial mass function of the stars can be measured through the metal abundance for variety of ions (Heger & Woosley 2010). Such studies are planned e.g. with the newly developing instruments on-board the Athena X-ray satellite, which is aiming to probe the GRB afterglow spectra, in combination with the studies in the quasar line of sight and probes of the Warm-Hot Intergalactic Medium.

The synthesized heavy elements can also be the source of a faint emission of a kind of an 'orphan' afterglow, if the main GRB jet is directed off-axis, or it is intrinsically very weak in its gamma ray fluence. Still, the detection of such an afterglow emission will be a hint of the existence of a black hole in the engine site. Measurements of nucleosynthesis products signatures may help constrain the model parameters for such engine, namely the black hole spin and its mass. The recent detections of the gravitational wave signal (Abbott et al. 2016) confirmed independently the existence of black holes in the Universe. The analysis of the gravitational wave signal allows to constrain the black hole mass and spin (with some uncertainty). In the case of the source GW150914, it was found that the signal is related to the merger of binary black hole. So far, the electromagnetic counterpart for this first event, was tentatively reported only by Fermi satellite, who gave a limit for detection of a weak gamma ray signal (Connaughton et al. 2016). No infrared emission was reported, and also the signal was not confirmed by other gamma-ray missions for the case of this burst (Greiner 2016).

Nevertheless, the detection of the electromagnetic counterpart of a gravitational wave source in the future events is appealing. The related estimates for the heavy elements synthesized in the ejecta could help constrain the parameters for the GRB engine, if the latter happens to coincide with the gravitational wave source. In particular, if the binary black holes merge within a remnant circumbinary disk, which is a leftover after the past supernova explosion (Perna et al. 2016), then the nucleosynthesis of elements within the disk engine and ejected winds can be responsible also for an infrared counterpart. Direct measurements of the escaping gamma-rays, which will be produced at larger distance in the r-process nucleosynthesis, are probably difficult with current X-ray and gamma-ray missions (Hotokezaka et al. 2016).

Table 2: Summary of the models with the massive black hole, $M_{\rm BH} = 62 M_\odot$, as estimated for the first LIGO-detected black hole. The mass of the torus is given in $M_\odot$, accretion rate in $M_\odot {\rm s}^{-1}$, the time is in seconds, and luminosity in erg s^{-1}.

Model	a	$R_{\rm max}$	$t_{\rm end}$	$M_{\rm t}(t=0)$	$M_{\rm t}(t_{\rm end})$	$< \dot{M} >$	$\dot{M}(t_{\rm end})$	$L_\nu^{\rm tot}(t_{\rm end})$	$L_{\rm BZ}(t_{\rm end})$
lbhAc	0.6	9.1	0.91	16.8	14.36	5.01	4.06	4.80×10^{53}	0
lbhBc	0.7	8.4	0.91	13.0	11.17	4.64	1.99	6.18×10^{53}	0
lbhCc	0.8	7.5	0.92	10.6	9.02	4.07	3.59	6.60×10^{53}	1.93×10^{51}
lbhDc	0.9	7.0	0.91	10.4	8.89	3.98	2.55	9.72×10^{53}	3.30×10^{51}
lbhEc	0.98	6.6	0.91	16.4	15.23	2.93	1.85	5.64×10^{54}	3.31×10^{52}

The black hole, which was the product of the merger of two black holes of about 29 and 36 Solar mass black holes, was also a moderately spinning one. The constraints for its dimensionless spin parameter obtained from the amplitude and phase evolution of the observed gravitational waveform gave a value of $0.67^{+0.05}_{-0.07}$, while the final black hole mass was equal to $62^{+4}_{-4}\ M_{\odot}$.

As can be shown, such a binary black hole merger, if accompanied by the matter accretion onto a rotating black hole, which happens either before, or after the merger, can lead to an unusual gamma ray burst (Janiuk et al. 2013b, 2017). In the case of the relatively small rate of the black hole rotation, such as in GW150914, the accretion will result in a very small electromagnetic flux dragged through the black hole horizon and hence negligibly small power of the Blandford-Znajek process.

We computed an additional set of the gamma ray burst engine models, with parameters taken to be representative for the above scenario (see Table 2). We have also computed the mass fraction distribution of heavy elements produced in this putative engine (Figure 12). We found, that contrary to the presented above 'fiducial' models, with a standard (small) black hole mass and accretion torus, here the nuclear conditions preferably lead to production of mainly Iron peak elements. In the model *lbhD* (see Table 2), the mass fraction of Iron 56 reached almost 1.0, while the isotopes from the group of Selenium and Manganese were 10^3 times less abundant. This result suggests a possible additional test for the conditions present in the GRB engine, e.g., if the event happened to be coincident with a merger of the two $\sim 30M_{\odot}$ black holes with masses of about $\sim 30M_{\odot}$ each. More generally, the gravitational waves discovery may reveal the new population of weak gamma ray bursts originating from the low Lorentz factor jets. In this case, the prompt electromagnetic emission may be difficult to discover, but the observation of a radioactive decay of elements produced in the engine of the GRB may be confronted with the engine simulation predictions. The black hole parameters, namely as its spin and mass, determine the shape of the gravitational wave signal.

Acknowledgments

We thank Szymon Charzynski, Petra Sukova, and Bartek Kaminski for helpful discussions, and Irek Janiuk for help in the MPI parallelization of the HARM-2D code. This research was supported in part by grant DEC-2012/05/E/ST9/03914 from the Polish National Science Center. We also acknowledge support from the Interdisciplinary Center for Mathematical Modeling of the Warsaw University, through the computational grants G53-5 and gb66-3.

REFERENCES

Abbott, et al., 2016, Phys. Rev. Lett., 116.061102

Abramowicz M.A., Jaroszynski M., Sikora M., 1978, *A&A*, **63**, 221

Barkov, M.V., Baushev, A.N., 2011, *New Astr.*, **16**, 46

Barkov, M.V., Komissarov, S.S., 2010 *MNRAS*, **401**, 1644

Blandford, R.D., Znajek, R.L., 1977, *MNRAS*, **179**, 433

Bromberg, O., Tchekhovskoy, A., 2016, *MNRAS*, **456**, 1739

Chen W.-X. & Beloborodov A., 2007, *ApJ*, **657**, 383

Connaughton V., et al., 2016, arXiv:1602.03920

Di Matteo T., Perna R., Narayan R., 2002, *ApJ*, **579**, 706

Fishbone L.G., Moncrief V., 1976, *ApJ*, **207**, 962

Fujimoto, S., Hashimoto, M., Arai, K., Matsuba, R., 2004, *ApJ*, **614**, 847

Gammie C.F., McKinney J.C. & Toth G., 2003, *ApJ*, **589**, 444

Goriely, S., Bauswein, A., Janka, H.-Th., 2011, *ApJ*, **738**, L32

Greiner, J., Burgess J. M., Savchenko V., Yu H.-F., 2016, *ApJ*, **827**, L38

Heger A., Woosley S.E., 2010, *ApJ*, **724**, 341

Hotokezaka, K.; Wanajo, S.; Tanaka, M.; Bamba, A.; Terada, Y.; Piran, T., 2016, *MNRAS*, **459**, 35

Ibanez, J.-M., Cordero-Carrin I., Aloy M.-A., Marti J.-M., Miralles J.-A., 2015, *Class Q. Grav*, **32**, 095007

Janiuk, A.; Perna, R., Di Matteo, T.; Czerny, B., 2004, *MNRAS*, **355**, 950

Janiuk A., Yuan Y.-F., Perna R., Di Matteo T., 2007, *ApJ*, **664**, 1011

Janiuk A., Yuan Y.-F., 2010, *A&A*, 509, 55

Janiuk A., Mioduszewski P., Moscibrodzka M., 2013, *ApJ*, **776**, 105

Janiuk A., Charzynski S., Bejger M.., 2013, *A&A*, **560**, 25

Janiuk A., 2014, *A&A*, **568**, 105

Janiuk A., Bejger M., Charzynski S., Sukova P., 2017, *New Astr.*, **51**, 7

Jonker P., O'Brien P., Amati L., et al., Supporting paper for the science theme "The Hot and Energetic Universe" to be implemented by the Athena+ X-ray observatory (http://www.the-athena-x-ray-observatory.eu), (arXiv:1306.2336)

Kohri, K., Mineshige, S., 2002, *ApJ*, **577**, 311

Kohri, K.; Narayan, R.; Piran, T., 2005 *ApJ*, **629**, 341

Kiuchi, K., Sekiguchi, Y., Kyutoku, K., Shibata, M., Taniguchi, K., Wada, T., 2015, *Phys. Rev. D*, **92**, 064034

Li, L.-X., Paczynski, B., 1998, *ApJ*, **507**, L59

Lopez-Camara D., Lee W.H., Ramirez-Ruiz E., 2009, *ApJ*, **692**, 804

Lee W.H., Ramirez-Ruiz E., 2007, *New Journal of Physics*, **9**, 17

Lee W.H., Ramirez-Ruiz E., Lopez-Camara D., 2009, *ApJ*, **699**, L93

Martin, D.; Perego, A.; Arcones, A.; Thielemann, F.-K.; Korobkin, O.; Rosswog, S., 2015, *ApJ*, **813**, 2

McKinney J.C., Gammie C.F., 2004, *ApJ*, **611**, 977

McKinney J.C., 2006, *MNRAS*, **368**, 1561

McKinney J.C., Blandford R., 2009, *MNRAS*, **394**, L126

McKinney J.C., Tchekhovskoy A., Blandford R. D., 2012, *MNRAS*, **423**, 3083

Moscibrodzka M., Falcke H., 2013, *A&A*, 559, L3

Noble S.C., Gammie C.F., McKinney J.C., & Del Zanna L., 2006, *ApJ*, **641**, 626

Paczynski B., 1998, *ApJL*, **494**, 45

Paschalidis V., Etienne Z., Liu Y.T., Shapiro S.L., 2011, *Phys. Rev. D*, **83**, 064002

Perna R., Lazzati D., Giacomazzo B., 2016, *ApJ*, **821**, L18

Piran T., 2005, *Reviews of Modern Physics*, **76**, 1143

Popham, R.; Woosley S.E.; Fryer, C., 1999, *ApJ*, **518**, 356

Reynoso, M. M.; Romero, G. E.; Sampayo, O. A., 2006, *A& A*, **454**, 11

Reddy S., Prakash M., Lattimer J.M., 1998, *Phys. Rev. D*, **58**, 013009

Schwab J., Shen, K.J., Quataert E., Dan M., Rosswog S., 2012, *MNRAS*, **427**, 190

Sekiguchi, Y., Kiuchi, K., Kyutoku, K., Shibata, M., 2015, *Phys. Rev D*, **91**, 064059

Shibata M., Sekiguchi Y., Takahashi R., 2007, *Progress of Theoretical Physics*, **118**, 2

Shibata M., Taniguchi K., 2011, *ApJL*, **734**, L36

Shibata M., Suwa Y., Kiuchi K., Ioka K., 2011, *Living Rev. in Relativity*, **14**, 6

Surman R., Caballero O.L., McLaughlin G.C., Just O., Janka H.-Th., 2014, *J. Phys. G*, **41**, 044006

Tanvir, N.R., Levan, A. J., Fruchter, A. S., Hjorth, J., Hounsell, R. A., Wiersema, K., Tunnicliffe, R. L. 2013, *Nature*, **500**, 547

Tchekhovskoy, A., McKinney, J.C., Narayan, R., 2008, *MNRAS*, **388**, 551

Wallerstein, G. et al., 1997, *Rev. Mod. Phys.*, **69**, 995

Woosley S.E., 1993, *ApJ*, **405**, 273

Yuan Y.-F., 2005, *Phys. Rev. D*, **72**, 013007

Zalamea I., Beloborodov A.M., *MNRAS*, **410**, 2302

This preprint was prepared with the AAS LaTeX macros v5.2.

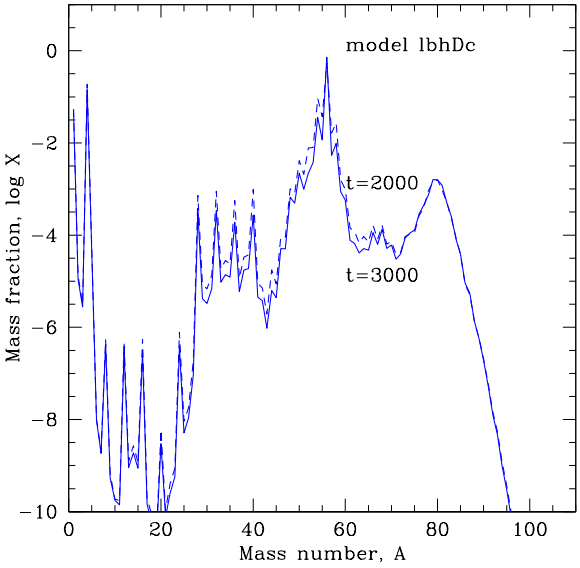

Fig. 12.— Heavy elements synthesized in the torus and its wind, for the model lbhDc in the Table 2. The black hole mass is $M_{\rm BH} = 62 M_\odot$, its spin is a=0.9, and torus mass is about 15 $M_\odot$.